Hypernuclear production by the (π^+,K^+) reaction

T. Motoba
Laboratory of Physics, Osaka Electro-Communication University, Neyagawa, Osaka 572, Japan

H. Bandō
Division of Mathematical Physics, Fukui University, Fukui 910, Japan

R. Wünsch
Central Institute for Nuclear Research, Rossendorf, Dresden, German Democratic Republic

J. Žofka
Nuclear Physics Institute, Czechoslovak Academy of Sciences, Řež-Prague, Czechoslovakia
(Received 6 January 1988)

The (π^+,K^+) strength functions (cross sections) are systematically calculated in the distorted-wave impulse approximation for the production of light-to-heavy hypernuclei: ${}^{12}_{\Lambda}$C, ${}^{16}_{\Lambda}$O, ${}^{28}_{\Lambda}$Si, ${}^{40}_{\Lambda}$Ca, ${}^{56}_{\Lambda}$Fe, ${}^{90}_{\Lambda}$Zr (and ${}^{208}_{\Lambda}$Pb). The quasifree continuum effects are taken into account in the frameworks of the Kapur-Peierls method and also of the continuum shell model. The characteristic feature of the (π^+,K^+) reaction is to provide well-separated series of peaks with high spin corresponding to the bound and resonant Λ states, yielding information on deep-lying hyperon states in heavy nuclei as well. Reasons for this effectiveness are clarified and discussed. The calculated results are in good agreement with the recent experiments which further demonstrates that the average Λ nucleus well can be simulated by an appropriate Woods-Saxon type potential ($V_0 \approx -30$ MeV) over a wide mass range of hypernuclei to a good approximation.

I. INTRODUCTION

Production of Λ and Σ hypernuclei has been performed mostly by the (K^-,π^-) reactions with the incident K^- meson in flight[1,2] or stopped.[3] The momentum of the K^- in flight has been usually chosen to approximately satisfy the recoilless condition, so that the substitutional states have been selectively populated in the produced hypernuclei. The analyses of the (K^-,π^-) reactions successfully applied the scheme presented in Ref. 4. In the stopped-K^- absorption, the produced hyperon gets a momentum comparable to the nucleon Fermi momentum ($p_F \approx 280$ MeV/c) and therefore nonsubstitutional states are appreciably populated as well.

In addition to the above K^--induced reactions, the feasibility and interest of the (π^+,K^+) reaction was theoretically proposed[5] and actually proved by the pioneering experiment ^{12}C$(\pi^+,K^+)^{12}_{\Lambda}$C done at Brookhaven.[6] With the pion momentum $p_\pi \approx 1040$ MeV/c chosen, the recoil momentum of Λ amounts to $q \approx 340$ MeV/c, which tends to favor the excitation of nonsubstitutional states and/or higher angular momentum configurations. In Ref. 7, the particular usefulness of the (π^+,K^+) reaction in studying medium and heavy Λ hypernuclei has been stressed and discussed in comparison with other methods. Recently the (π^+,K^+) experiments have been further extended at the Brookhaven National Laboratory (BNL) to cover light-to-heavy hypernuclei.[8]

The (π^+,K^+) reaction is now going to be applied also at the National Laboratory for High Energy Physics (KEK) for study of Λ and, we hope, Σ hypernuclei. Interests are not only in the structure of light hypernuclei but also in the deep hyperon orbitals in heavy hypernuclei. Also, some coincidence experiments as well as singles are planned, of which, particularly pertinent to (π^+,K^+) reaction, is the production of polarized hypernuclei followed by measurement of angular correlations of their weak decay products or measurement of the Λ magnetic moment in nucleus.[9]

In order to obtain a realistic excitation spectrum for hypernuclear production, it is necessary to take into account quasifree continuum effects, since in many cases states of interest are observed above the hyperon threshold.[10,11] For this purpose the continuum shell model[12] (CSM) has been applied to the (K^-,π^-) Λ-hypernuclear production process.[13] As for the (π^+,K^+) reaction, only one application of CSM has been made for the ${}^{12}_{\Lambda}$C production.[14] For the Σ-hypernuclear production, several theoretical attempts including CSM have been made to evaluate quasifree contributions in connection with the puzzling narrow Σ states.[15–19]

In this paper, responding to the challenge of new (π^+,K^+) data,[8] we calculate the strength functions for light-to-heavy Λ-hypernucleus productions by including the quasifree continuum effects and analyze their properties. We adopt the Kapur-Peierls (K-P) method,[20] in addition to CSM, to treat the continuum effects. The calculations have been performed in the framework of the distorted-wave impulse approximation (DWIA). In Sec. II both the K-P method and CSM are briefly described. The characteristics of the (π^+,K^+) reaction are summa-

rized in Sec. III, where emphasis is put on the possibility of observing deep hyperon single-particle states and the comparison between the (π^+,K^+) and (stopped K^-,π^-) reactions on typical targets (^{56}Fe and ^{208}Pb). In Sec. IV, calculated results of the strength functions are presented for the (π^+,K^+) productions of

$$^{56}_{\Lambda}\text{Fe},\ ^{90}_{\Lambda}\text{Zr},\ ^{40}_{\Lambda}\text{Ca},\ ^{28}_{\Lambda}\text{Si},\ ^{16}_{\Lambda}\text{O},\ \text{and}\ ^{12}_{\Lambda}\text{C}$$

in this order. They include hyperon resonances and quasifree contributions and are discussed in comparison with the recent experimental data. Concluding remarks are given in Sec. V.

II. STRENGTH FUNCTION WITH CONTINUUM EFFECTS

We consider the (π,K^+) reaction on the target nucleus $^AZ(J_i)$ at K^+ forward angles ($\theta=0°$). Then the spin-flip component of the reaction can be neglected and the differential cross section in the distorted-wave impulse approximation is expressed as

$$\frac{d^2\sigma(E_Y,\theta)}{dE_Y d\Omega_L}=\alpha\frac{d\sigma_f(\theta)}{d\Omega_L}S(E_Y,\theta)\ , \tag{2.1}$$

where $d\sigma_f/d\Omega$ is the cross section of the elementary $\pi N\rightarrow YK^+$ process in the laboratory system and α is a kinematical factor accounting for the transformation from the two-body to many-body laboratory systems. When considering forward-angle reactions and neglecting spin-flip term, it may be simply factored,[5] otherwise a nontrivial mixing of both spin-nonflip f and spin-flip g amplitudes appears. The strength function (response function) $S(E_Y,\theta)$ is a function of the final hypernuclear state energy which is given in this paper by the energy E_Y relative to the hyperon (Y) escape threshold.

To evaluate the strength function $S(E_Y,\theta)$, we mainly apply the Kapur-Peierls–type method[20] and additionally the continuum shell model.[12,13,18] Details of both methods as applied here are suppressed for the sake of brevity and may be found in Ref. 21.

A. The Kapur-Peierls–type treatment

In the K-P method, the outgoing boundary condition is imposed at the channel radius r_c on the hyperon wave function. The expression for $S(E_Y,\theta)$ in K-P reads

$$S(E_Y,\theta)=-\frac{1}{\pi}\sum_J\sum_\mu \mathrm{Im}\left[\frac{N_{J,\mu}(E_Y,\theta)}{E_Y-E_{J,\mu}(E_Y)}\right]\ , \tag{2.2}$$

where J is the angular momentum of the final hypernuclear state and $N_{J,\mu}$ is the "effective neutron number" given below. $E_{J,\mu}(E_Y)$ is the μth eigenenergy with the eigenfunction $\Psi_{J,\mu}(E_Y)$ of the Hamiltonian $\tilde{H}$ which includes the Bloch operator[20] to account for the outgoing boundary condition at appropriate channel radius r_c.

The transition operator $\hat{T}(\theta)$ in the (π^+,K^+) reaction is given by

$$\hat{T}_{\pi K}(\theta)=\int d^3\mathbf{r}\chi^{(-)*}_{\mathbf{p}_K}(\mathbf{r})\chi^{(+)}_{\mathbf{p}_\pi}(\mathbf{r})\sum_{i=1}^{A}u_-(i)\delta(\mathbf{r}-\mathbf{r}_i) \tag{2.3}$$

with the operator $u_-(i)$ converting ith nucleon into a hyperon and χ's being the meson distorted waves. The effective nucleon number $N_{J,\mu}$ in Eq. (2.2) is defined as

$$N_{J,\mu}(E_Y,\theta)=\langle\Phi_0\,|\,\hat{T}^\dagger(\theta)\,|\,\Psi_{J,\mu}(E_Y)\rangle \times\langle\tilde{\Psi}_{J,\mu}(E_Y)\,|\,\hat{T}(\theta)\,|\,\Phi_0\rangle\ , \tag{2.4}$$

where Φ_0 denotes the ground-state wave function of the target nucleus and $\tilde{\Psi}$ is adjoint of Ψ. Note that $N_{J,\mu}$ and $E_{J,\mu}$ are both complex numbers.

For some hypernuclei the strength functions of the (stopped K^-,π^-) process is also evaluated for comparison with the (π^+,K^+) process. In this case, we use the transition operator $\hat{T}_{\text{stop-}K}$ defined by the product of K^- atomic orbital and outgoing π^- wave functions,

$$\chi^{(-)*}_{\mathbf{p}_\pi}(\mathbf{r})R^K_{nl}(r)Y_{lm}(\hat{\mathbf{r}})\ ,$$

instead of $\chi^{(-)*}_{\mathbf{p}_K}(\mathbf{r})\chi^{(+)}_{\mathbf{p}_\pi}(\mathbf{r})$ in Eq. (2.3).

For the bound states with $E_Y<0$, the strength function $S(E_Y;\theta)$ of Eq. (2.2) should be a δ function multiplied by the effective nucleon number $N_{J,\mu}$. Thus, $S(E_Y;\theta)$ includes not only the production of hypernuclear bound states but also the effect of continuum states. The latter actually consists of contributions from hyperon resonances and quasifree processes (QF).

B. The continuum shell model

In CSM,[13,18] the calculation is performed in the Woods-Saxon basis, which consists of a discrete part of bound states and of a continuous part of unbound or scattering states. An unbound many-body nuclear state $\psi_{E,f}$ with excitation energy E decaying into channel f is expanded in this basis. The whole configuration space employed in CSM includes configurations (ϕ_R) with all A baryons in bound states (Q subspace) and configurations with some baryons in scattering states (P subspace). In fact, present CSM is restricted to configurations with a single particle in the continuum.

It may happen that the continuous single-particle spectrum exhibits a resonant behavior (shape resonance). In this case, a single-particle resonance state is defined with a wave function cut off at a distance r_c (analog to the channel radius of the K-P method). The oscillating tail of the quasibound state is healed out by the same Bloch operator as in the K-P method. Many-body configurations in which a particle occupies such a resonance or "quasibound" state is then also included in the Q subspace and the projector $\hat{Q}$ is extended correspondingly. A double counting is avoided by keeping $\hat{P}$ complementary: $\hat{P}=1-\hat{Q}$.

The CSM is related to the K-P method in the following manner: Defining more and more "quasibound" states by an appropriate boundary condition and adding them to the Q subspace, the remaining component becomes smaller and smaller. In the limit of an infinite number of quasibound states, all the continuous spectrum would be fully described by the resonance terms. Then, the remaining difference would be the single-particle basis and the discretization procedure (which is physical in

CSM and a formal expansion in K-P method).

In the actual CSM calculation, only those single-particle resonances are included in the resonance term which give rise to pronounced bumps in the corresponding excitation function. In this case, the poles of the propagator which are defined by the eigenvalues of the effective Hamiltonian H_{QQ}^{eff} describe the positions E_ν and widths Γ_ν of the many-body resonances

$$\langle \phi_\nu^* \mid H_{QQ}^{\text{eff}} \mid \phi_{\nu'} \rangle = (E_\nu - i\Gamma_\nu/2)\delta_{\nu\nu'} , \tag{2.5}$$

$$H_{QQ}^{\text{eff}} = \hat{Q}\mathbf{H}\hat{Q} + \hat{Q}\mathbf{H}\frac{\hat{P}}{E^+ - \hat{P}\mathbf{H}\hat{P}}\mathbf{H}\hat{Q}, \quad E^+ = E + i\eta . \tag{2.6}$$

The full Hamiltonian $\mathbf{H}$ includes a contact residual interaction. The matrix element $\langle \phi_\nu \mid \hat{T}(\theta) \mid \phi_0 \rangle$ determines the effective neutron number for the resonant excited state described by the wave function ϕ_ν.

C. Folding of the strength functions

In Sec. IV we display the strength function $S_\Gamma(E_Y,\theta)$ obtained by folding $S(E_Y,\theta)$ with Gaussian or Lorentzian shapes with a width Γ which is to take account of the experimental resolution (present or improved one in the future) and some spreading of the N-hole strengths. The folding procedure is as follows ($E = E_Y$):

Gaussian:

$$f^{(G)}(E;E_i) = \frac{2}{\sqrt{\pi}\Gamma_i}\exp[-(E-E_i)^2/(\Gamma_i/2)^2] , \tag{2.7}$$

Lorentzian:

$$f^{(L)}(E;E_i) = \frac{\Gamma_i}{2\pi}\frac{1}{(E-E_i)^2+(\Gamma_i/2)^2} , \tag{2.8}$$

$$S_\Gamma(E) = \int S(E_i) f(E;E_i) dE_i . \tag{2.9}$$

D. Parameters of the eikonal approximation

In the present calculation the meson distorted waves are evaluated under the eikonal approximation (details of which are described in Ref. 7) by employing the empirical meson-nucleon total cross sections:[22]

(π^+,K^+): $\bar{\sigma}(\pi^+N) = 41$ mb and $\bar{\sigma}(K^+N) = 14$ mb ,

$(p_\pi = 1040$ MeV/c, $\theta_K \approx 0°)$,

(stopped K^-,π^-): $\bar{\sigma}(\pi^-N) = 120$ mb ,

(K^-,π^-): $\bar{\sigma}(K^-N) = 30$ mb and $\bar{\sigma}(\pi^-N) = 30$ mb ,

$(p_K = 720$ MeV/c, $\theta_\pi \approx 0°)$.

The treatment of meson distortions in the eikonal approximation may be further improved[23] by generating meson wave functions so as to fit the corresponding scattering data, but it should not be decisive for the present analysis.

III. CHARACTERISTICS OF THE (π^+,K^+) REACTION

In order to illustrate the characteristic feature of the (π^+,K^+) reaction, here we show the calculated excitation spectra for the $^{56}_{\Lambda}$Fe and $^{208}_{\Lambda}$Pb production in comparison with those of the (K^-,π^-) and (stopped K^-,π^-) reactions. For the sake of clarity, the excitation spectra in this section do not include continuum effects.

Figure 1 compares the calculated excitation spectra for three processes producing $^{56}_{\Lambda}$Fe. The target wave function is assumed to be described with the two-hole two-particle state

$$[(0f_{7/2})_P^{-2}(1p_{3/2})_N^2] ,$$

with respect to the closed configuration up to the $0f_{7/2}$

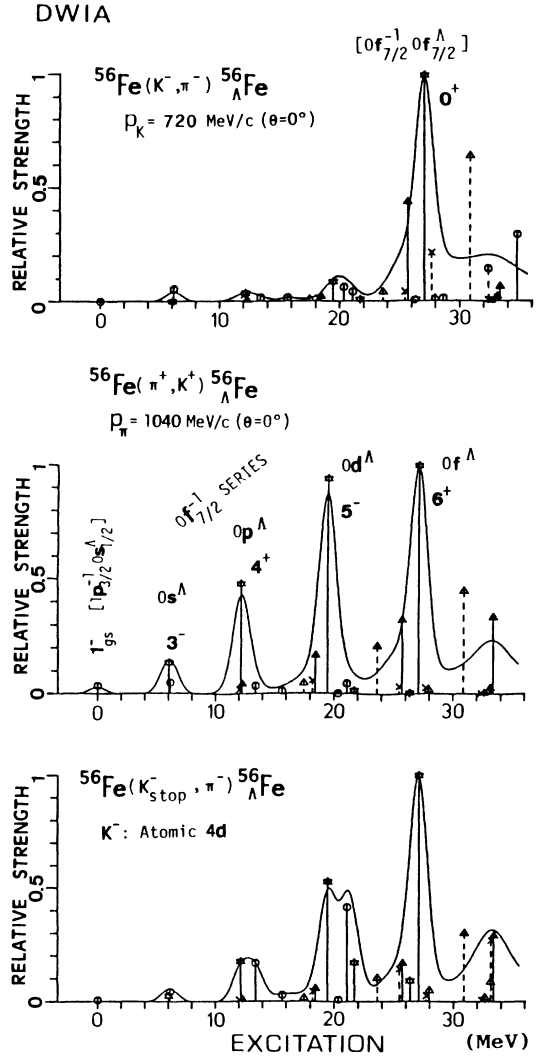

FIG. 1. Comparison of three DWIA spectra for the $^{56}_{\Lambda}$Fe production. The abscissa is excitation energy (in MeV) with respect to the hypernuclear ground state $1^-_{\text{g.s.}}$ which corresponds to $E_\Lambda = -B_\Lambda \approx -20.8$ MeV. The line spectra are folded with $\Gamma = 2$ MeV Gaussian shape. The neutron-hole states are labeled as $1p_{3/2}^{-1}$ (open circle), $0f_{7/2}^{-1}$ (star), $0d_{3/2}^{-1}$ (solid triangle), $0d_{5/2}^{-1}$ (open triangle), etc.

orbit. Here, neglecting small p-h interaction $v(N^{-1}\Lambda)$ and small Λ spin-orbit splittings, the effective neutron numbers summed over $j_\Lambda = l_\Lambda \pm \frac{1}{2}$ and J are plotted in relative scale as a function of $E_\Lambda = -B_\Lambda$. Each strength is folded with Gaussian of width $\Gamma = 2$ MeV for the p-h configuration with the surface neutron hole $j_N^{-1} = (1p_{3/2}, 0f_{7/2})_N^{-1}$ and $\Gamma = 4$ MeV for deeper neutron holes with the excitation energy $E_N^* > 15$ MeV.

In contrast to the exclusive excitation of the substitutional states in the in-flight (K^-,π^-) reaction, a series of well-separated peaks are obtained in the (π^+,K^+) reaction as shown in Fig. 1. This is primarily due to the large transferred momentum $q \approx 330$ MeV/c at $p_\pi = 1040$ MeV/c. The (π^+,K^+) spectrum is more selective and simpler than that of the (stopped K^-,π^-) reaction which also involves a sizable momentum transfer of $q \approx 280$ MeV/c. The characteristic difference between these two processes becomes more drastic in a heavier target ^{208}Pb as seen in Fig. 2. In the ^{208}Pb (stopped $K^-,\pi^-)^{208}_\Lambda$Pb reaction, many states are rather equally excited and constitute a dense and almost structureless spectrum, so that it might be difficult to see particular states in a distinguishable way.

Figure 3 displays J-separated contributions to the strongest two peaks of $^{56}_\Lambda$Fe. In (π^+,K^+), a specific p-h coupling plays a dominant role in each strong peak, while in (stopped K^-,π^-) various p-h angular momenta contribute comparably. The (K^-,π^-) reaction in flight would not populate appreciably nonsubstitutional states of the second group.

Recently the ^{56}Fe$(\pi^+,K^+)^{56}_\Lambda$Fe experiment was performed at KEK (Ref. 24) and the preliminary analysis seems to be consistent with our prediction. Moreover, the calculated spectrum may be compared indirectly with the recent BNL data of the ^{51}V$(\pi^+,K^+)^{51}_\Lambda$V reaction,[8] since this target has also the neutron closed $0f_{7/2}$ orbit. In the data one observes several peaks suggesting the $f_{7/2}$-hole series shown above.

From the above two examples, one may understand how the (π^+,K^+) reaction is selective in character and useful to provide empirical information on deep hyperon orbits in heavy hypernuclei. Now we summarize the characteristic features of the (π^+,K^+) reaction.

(i) A series of the $[(n_N l_N j_N)^{-1}(n_Y l_Y j_Y)]_J$ configurations with $n_N = n_Y = 0$, large l and large J are selectively excited. The selectivity comes from the fact that the effective neutron number N_J is related to a unique partial wave $\tilde{j}_J$ involving large momentum

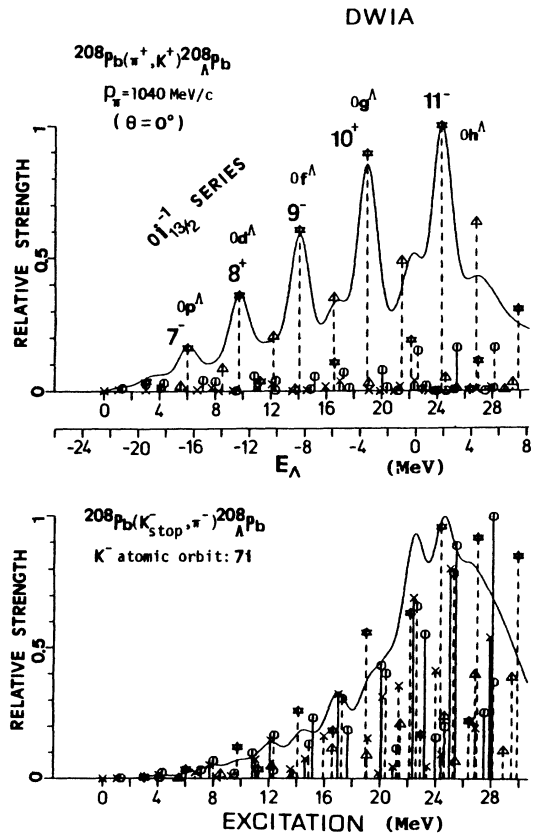

FIG. 2. The (π^+,K^+) and (stopped K^-,π^-) spectra for the $^{208}_\Lambda$Pb production calculated in DWIA. The line spectra are folded with $\Gamma = 2$ MeV Gaussian shape. The neutron-hole states are labeled as $2p^{-1}$ (plus), $1f^{-1}$ (open circle), $0i^{-1}_{13/2}$ (star), $0h^{-1}_{9/2}$ (open triangle), etc.

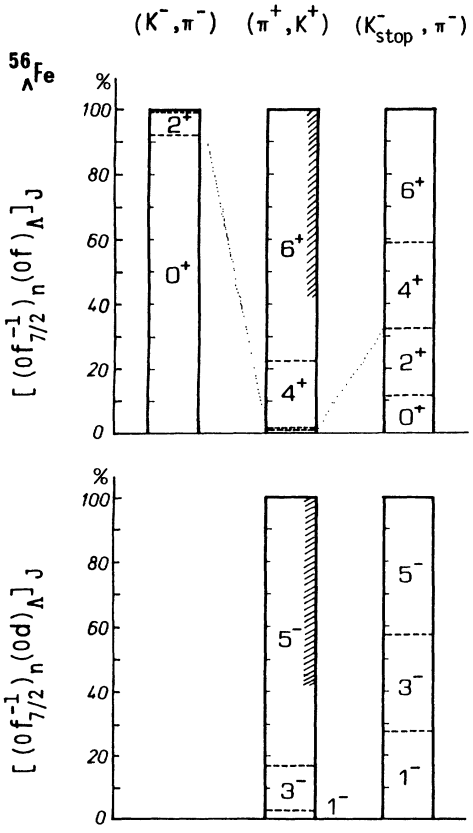

FIG. 3. Separate contributions (in %) to the large peaks in different processes leading to the $^{56}_\Lambda$Fe production. The hatched part indicates the contribution from the $[j_>^{-1} j_<^\Lambda]_{J=J_{max}}$ combination.

transfer.

(ii) The particular combinations with stretched angular momentum and natural parity,

$$[(j_>^{-1})_N(j_<)_\Lambda]_{J_{\max}} \text{ and } [(j_<^{-1})_N(j_>)_\Lambda]_{J_{\max}} ,$$

prevail in the peaks.

(iii) The excitation of high-l_Y states is important for their possibility of observing because, even above the hyperon escape threshold, the high centrifugal barrier keeps the peaks quite narrow.

IV. RESULTS ON THE STRENGTH FUNCTIONS AND DISCUSSION

In this section we present the strength functions including continuum effects for the productions of ${}^{56}_{\Lambda}$Fe, ${}^{90}_{\Lambda}$Zr, ${}^{40}_{\Lambda}$Ca, ${}^{28}_{\Lambda}$Si, ${}^{16}_{\Lambda}$O, and ${}^{12}_{\Lambda}$C in this order. They are mostly based on the Kapur-Peierls method because essentially the same results are obtained with CSM. In describing hypernuclear states we use N-hole Λ-particle basis

$$[N^{-1}\Lambda]_J=[(n_N l_N j_N)^{-1}(n_\Lambda l_\Lambda j_\Lambda)]_J ,$$

and to generate the single-particle wave functions (nlj), we adopt the Woods-Saxon potential:

$$U=(V_0+iW_0)f(r) + V_{\rm SO}\left[\frac{\hbar}{m_\pi c}\right]^2\frac{1}{r}\frac{df(r)}{dr}(\boldsymbol{l}\cdot\boldsymbol{\sigma})+V_{\rm Coulomb} , \quad (4.1)$$

$$f(r)=\{1+\exp[(r-R)/a]\}^{-1} . \quad (4.2)$$

The potential parameters for Λ hyperon are chosen as

$$R_\Lambda=1.1(A-1)^{1/3}\text{ fm},\quad a_\Lambda=0.60\text{ fm} ,$$

$$V_0^\Lambda=-30\text{ MeV},\quad V_{\rm SO}^\Lambda=2.0\text{ MeV},\quad W_0^\Lambda=0\text{ MeV} .$$

Here we assume small Λ spin-orbit (SO) potential, which was suggested by the previous (K^-,π^-) data.[1] Table I lists the Λ single-particle energies calculated with this Woods-Saxon potential. In Table II, the adopted single-neutron orbits are listed. The single-neutron energies in Table II are simulated by the Woods-Saxon potential with

$$R_N=1.25A^{1/3}\text{ fm},\quad a_N=0.53\text{ fm} ,$$

$$V_0^N=-50\text{ MeV},\quad V_{\rm SO}^N=7.0\text{ MeV},\quad W_0^N=0\text{ MeV} ,$$

but in some cases the empirical values are employed.

Since the major part of the ΛN interaction v_{YN} is taken into account by the above Woods-Saxon potential U_Y, we assume here that the residual ΛN interactions are small and negligible for the present purpose. In the CSM calculations, however, the δ-type ΛN residual interaction is introduced and it is seen that the effect of the mixing on the overall shape of spectra is not big, but it could be distinguished when the experimental resolution is largely improved.

A. The ^{56}Fe$(\pi^+,K^+)^{56}_{\Lambda}$Fe reaction

All the spectra have been calculated in DWIA, but a comparison with plane-wave impulse (PWIA) approximation is useful for better insight into the mechanism of production. The patterns of the PWIA and DWIA spectra look quite similar, while the meson distortion-absorption effects reduce the absolute values of the production cross section to 10–17 % of the PWIA estimate. It is interesting to note that, in general, the low-spin partial waves are more reduced by the meson absorption than the high-spin ones. As a result, the peaks in the DWIA strength function tend to become "sharp" and pronounced due to the reduction of the shoulder and tail made up of the nonselective low-spin states.

TABLE I. Calculated single-particle bound energies of Λ in the Woods-Saxon potential given in the text. The positive energies in parentheses indicate sharp resonance states obtained near the Λ escape threshold. All entries are in MeV.

		${}^{208}_{\Lambda}$Pb	${}^{90}_{\Lambda}$Zr	${}^{56}_{\Lambda}$Fe	${}^{40}_{\Lambda}$Ca	${}^{28}_{\Lambda}$Si	${}^{16}_{\Lambda}$O	${}^{12}_{\Lambda}$C
	$0s_{1/2}$	−25.9	−23.0	−20.8	−19.0	−16.8	−13.0	−10.4
	$0p_{3/2}$	−21.9	−16.9	−13.3	−10.5	−7.4	−2.7	−0.3
ε_Λ	$0p_{1/2}$	−21.7	−16.5	−12.6	−9.6	−6.3	−1.5	(0.3)
	$0d_{5/2}$	−17.2	−10.2	−5.2	−1.9	(1.2)		
	$0d_{3/2}$	−16.8	−9.1	−3.9	−0.4	(2.4)		
	$1s_{1/2}$	−15.4	−8.1	−3.8	−1.4			
	$0f_{7/2}$	−12.0	−2.8	(2.4)				
	$0f_{5/2}$	−11.2	−1.3	(4.0)				
	$1p_{3/2}$	−9.5	−1.3					
	$1p_{1/2}$	−9.2	−0.9					
	$0g_{9/2}$	−6.2						
	$0g_{7/2}$	−5.1						
	$1d_{5/2}$	−3.6						
	$1d_{3/2}$	−3.0						
	$2s_{1/2}$	−2.8						
	$0h_{11/2}$	−0.2						
	$0h_{9/2}$	(1.4)						

TABLE II. The single-neutron energies (ε_N) employed in the calculation of strength functions. All entries are in MeV.

		$^{90}_{\Lambda}$Zr	$^{56}_{\Lambda}$Fe		$^{40}_{\Lambda}$Ca	$^{28}_{\Lambda}$Si	$^{16}_{\Lambda}$O	$^{12}_{\Lambda}$C
	$0d_{5/2}$		−23.2	$0s_{1/2}$			−35.0	−34.0
	$1s_{1/2}$		−20.0	$0p_{3/2}$	−44.0	−29.6	−20.9	−17.6
ε_N	$0d_{3/2}$		−19.2	$0p_{1/2}$	−38.0	−25.4	−14.8	
	$0f_{7/2}$	−22.5	−13.3	$0d_{5/2}$	−21.1	−16.0		
	$1p_{3/2}$	−16.5	−8.4	$1s_{1/2}$	−18.1			
	$0f_{5/2}$	−16.9		$0d_{3/2}$	−15.6			
	$1p_{1/2}$	−14.6						
	$0g_{9/2}$	−12.4						

In order to visualize features with higher and lower resolution, we display two DWIA spectra with $\Gamma=1$ and 3 MeV Lorentzian widths in Fig. 4, where the pronounced peaks are based on the $0f_{7/2N}$-hole configuration. Although the fragmentation of nucleon-hole strengths are not included here, the $\Gamma=1$ MeV spectrum shows a possibility of fixing the Λ spin-orbit splittings (e.g., $d_{5/2}-d_{3/2}$) if the real V_{SO}^{Λ} is near the adopted value. With $\Gamma=3$ MeV, the valleys between Λ major-shell peaks become shallower and, in addition, the ground-state peak almost smears. This figure thus illustrates how desirable are experimental attempts to improve the resolution beyond the presently achieved value of $\Gamma\approx 3$ MeV.

It should be noted that the big peak at $E_\Lambda\approx 8$ MeV corresponding to the $[0f_{7/2N}^{-1}0f_\Lambda]_{J\approx J_{max}}$ state in Fig. 1 (middle) consists of the 6^+ and 4^+ sharp resonances in the continuum as shown by dashed QF curves in Fig. 4. As the nuclear core part (^{55}Fe) is excited in this series of peaks ($0f_{7/2}^{-1}$ instead of $1p_{3/2}^{-1}$), i.e.,

$$E_N^*(\tfrac{7}{2}^-;{}^{55}\mathrm{Fe})^{\mathrm{cal}}=4.9\ \mathrm{MeV}\ ,$$

the actual escape threshold for Λ is shifted up to $E_\Lambda=0+E_N^*=4.9$ MeV. In addition to this, the high centrifugal barrier for $0f_\Lambda$ supports the realization of the "high-lying" sharp resonance. Moreover, the width arising from the coupling with

$$[(1p_{3/2}^{-1})_N(nl)_\Lambda]_{J=J_{max}}$$

state having lower threshold is very small, as the $N^{-1}\Lambda$ interaction for such a high J is extremely weak. The peak at $E_\Lambda\approx 8$ MeV, however, becomes a little broader due to the overlap with the adjacent deeper hole states

$$[0d_{3/2N}^{-1}0d_\Lambda]_{4^+},\ [0d_{5/2N}^{-1}0d_\Lambda]_{4^+},\ \text{etc.}$$

With the chosen Woods-Saxon potential the ground 1^- state is obtained at $E_\Lambda=-20.8$ MeV, while the predicted energies of the above series of peaks are

$$E_\Lambda=-16.3(J=3^-),\ -8.1(4^+),\ 0.7(5^-)\ ,$$
$$\text{and } 7\text{–}10\ \mathrm{MeV}(6^+\text{ and }4^+)\ ,$$

respectively. The present calculation thus suggests $\hbar\omega_\Lambda\approx 8$ MeV for the Λ-particle major-shell energy interval.

In Fig. 5 is displayed the $\theta=10°$ strength function ob-

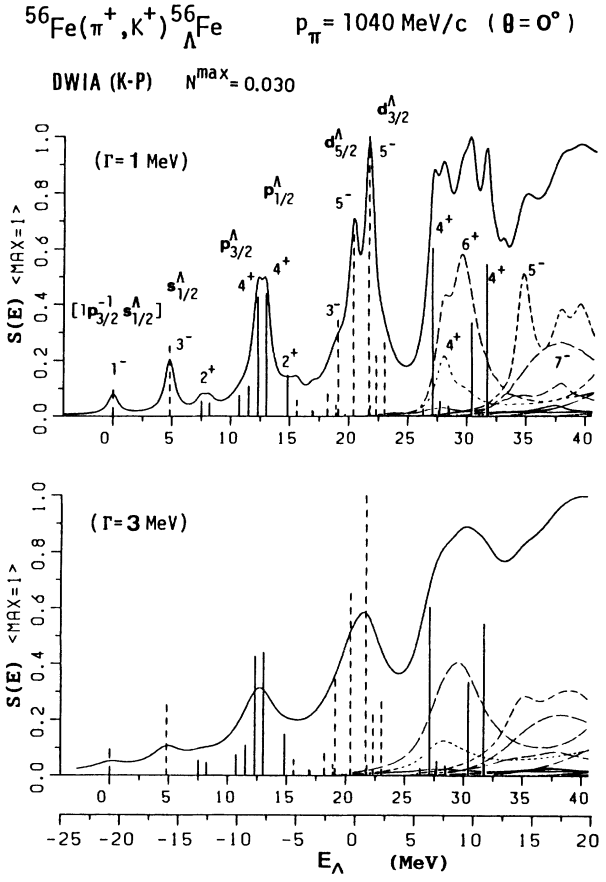

FIG. 4. Strength functions $S_\Gamma(E_\Lambda;\theta=0°)$ for the ^{56}Fe$(\pi^+,K^+)^{56}_{\Lambda}$Fe reaction with $p_\pi=1040$ MeV/c calculated with the K-P method. The lengths of solid and dashed lines are proportional to the J-summed effective neutron numbers, $\sum_J N_{\mathrm{eff}}[j_N^{-1}j_\Lambda]_J$, for positive-parity and negative-parity p-h states, respectively. Some pronounced peaks are indicated by j_Λ and J_{max} for the structures. N^{max} means the maximum effective neutron number for the bound p-h states. The strength function is drawn as normalized to the maximum value within the indicated energy range E_Λ. The resonance and quasifree contributions with various angular momenta are shown by dashed curves ($E_\Lambda>0$). The folding is made with Lorentzian width of $\Gamma=1$ MeV (top) and $\Gamma=3$ MeV (bottom).

tained by the CSM method where the accumulated continuum contributions from various neutron-hole configurations are shown to much higher energy. This spectrum is folded with the $\Gamma=3$ MeV Lorentzian and hence the $E_\Lambda<20$ MeV part should be compared with the $\Gamma=3$ MeV K-P result shown in Fig. 4 (bottom). Note that the difference in transferred momentum q for $\theta=0°$ and 10° at $p_\pi\approx1050$ MeV/c is much less than 10%. The comparison reveals close similarity between the two spectra in spite of quite a difference in the methods and of inclusion of residual contact interaction.

Using the empirical lab. cross section[5] $\alpha(d\sigma/d\Omega)=500\mu$b/sr for the elementary process $\pi^+N\to\Lambda K^+$, the DWIA cross sections for the peaks at $E_\Lambda=-8$ and 0 MeV are calculated to be

$$\frac{d\sigma}{d\Omega}[0f_{7/2N}^{-1}0p_\Lambda]=13\ \mu\text{b/sr}\quad(\theta=0°)\ ,$$

and

$$\frac{d\sigma}{d\Omega}[0f_{7/2N}^{-1}0d_\Lambda]=25\ \mu\text{b/sr}\quad(\theta=0°)\ ,$$

respectively. The DWIA effective neutron numbers for the typical p-h states are summarized in Table III, whereas the differential cross sections for typical states are discussed in the text.

In connection with the use of the value 500 μb/sr for the many-body lab differential cross section, four remarks are due in order to illustrate its uncertainty of some 10–20%. The elementary differential cross sections at small angles bear large experimental errors and it makes the precise extrapolation difficult. The inclusion of the Fermi motion of nucleons in the target (via the Fermi averaging[23] or another more precise procedure[25]) would lower the value of $d\sigma/d\Omega$ slightly. The factor α characterizing the off-shell extension of the two-body process as used in Ref. 5 is necessarily an approximation. The experimental angle has appreciable range (±2°–4°). Thus, instead of attempting to precise partially some of above influences, we prefer to employ some representative value and 500 μb/sr has been thus chosen.

B. ^{90}Zr(π^+,K^+)$^{90}_\Lambda$Zr versus the ^{89}Y(π^+,K^+)$^{89}_\Lambda$Y experiment

Figure 6 displays the calculated (π^+,K^+) strength functions ($\Gamma=2$ MeV) for a typical heavy hypernucleus $^{90}_\Lambda$Zr. The obtained series of well-separated peaks is attributed to the configurations:

$$[(0g_{9/2}^{-1})_N(nl)_\Lambda]_J$$

with

$$nl(J)=0s_\Lambda(4^+_{\text{g.s.}};100\%)\text{ at }E_\Lambda^{\text{cal}}=-23.0\text{ MeV}\ ,$$
$$0p_\Lambda(5^-;81.3\%)\text{ at }-16.7\text{ MeV}\ ,$$
$$0d_\Lambda(6^+;77.3\%)\text{ at }-9.3\text{ MeV}\ ,$$
$$0f_\Lambda(7^-;72.6\%)\text{ at }-1.3\text{ MeV}\ .$$

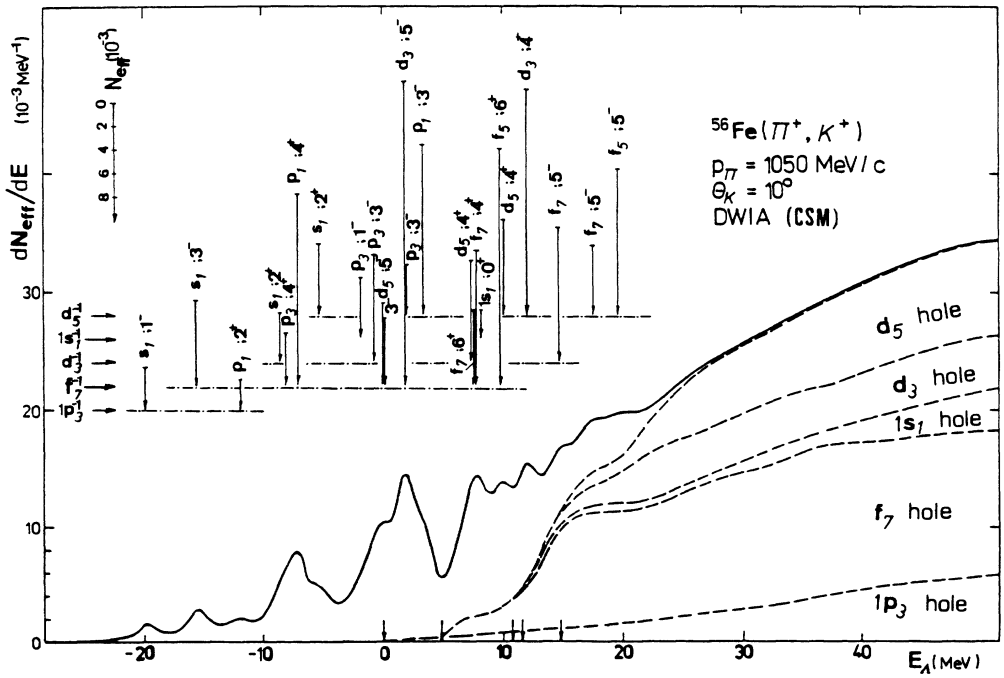

FIG. 5. The continuum shell-model result of the strength function $S_\Gamma(E_\Lambda;\theta=10°)$ for ^{56}Fe(π^+,K^+)$^{56}_\Lambda$Fe with $p_\pi=1050$ MeV/c, which is folded with Lorentzian width $\Gamma=3$ MeV. The hole thresholds are indicated by arrows at the bottom axis. The top insertions sketch the line spectrum of the effective neutron number for p-h state characterized by $[j_N^{-1}j_\Lambda]J$, where bars end at corresponding hole levels indicated by horizontal arrows on the left-hand side. The notations are used as f_7 for $0f_{7/2}$, p_3 for $0p_{3/2}$, etc. Long dashed curves at $E_\Lambda>0$ give contributions of various open channels.

TABLE III. The DWIA estimates of the effective neutron numbers of the forward angle (π^+,K^+) reaction leading to the indicated p-h states: $[j_N^{-1}j_\Lambda]$. All entries are $N_{\rm eff}\times 10^3$ at $\theta=0°$. In the $^{56}_{\Lambda}$Fe case, the PWIA values are also listed in the square brackets [ ].

j_Λ	$^{208}_{\Lambda}$Pb $0i_{13/2}^{-1}$	$^{90}_{\Lambda}$Zr $0g_{9/2}^{-1}$	$^{56}_{\Lambda}$Fe $0f_{7/2}^{-1}$[PW]	$^{40}_{\Lambda}$Ca $0d_{3/2}^{-1}(0d_{5/2}^{-1})$	$^{28}_{\Lambda}$Si $0d_{5/2}^{-1}$	$^{16}_{\Lambda}$O $0p_{1/2}^{-1}(0p_{3/2}^{-1})$	$^{12}_{\Lambda}$C $0p_{3/2}^{-1}$
$0s_{1/2}$	1.4	3.4	7.4[81.3]	6.0(7.9)	17.7	9.8(17.0)	34.9
$0p_{3/2}$	2.9	7.3	12.6[97.1]	17.9(11.2)	22.9	20.6(19.2)	36.6
$0p_{1/2}$	3.1	6.7	13.0[109.0]	0.4(13.1)	24.7	0.5(16.0)	
$0d_{5/2}$	4.8	11.6	19.2[139.1]	33.3(15.1)			
$0d_{3/2}$	8.5	17.9	29.5[183.8]	1.6(23.0)			
$1s_{1/2}$	1.4	2.3	1.1[9.0]	0.8(1.3)			
$0f_{7/2}$	7.5	17.1					
$0f_{5/2}$	14.9	32.2					
$1p_{3/2}$	1.7	2.9					
$1p_{1/2}$	2.2	2.2					
$0g_{9/2}$	10.5						
$0g_{7/2}$	22.5						
$1d_{5/2}$	2.5						
$1d_{3/2}$	4.6						
$2s_{1/2}$	0.3						
$0h_{11/2}$	12.5						
$0h_{9/2}$	24.4						

The percentage indicates the share of the stretched angular momentum contribution to each peak and again exhibits the high selectivity. The fifth peak obtained in the continuum ($E_\Lambda=4$–9 MeV) consists of three sharp resonances (mainly $J=8^+$ and 6^+) and the "bound-state peak" of

$$[(0f_{7/2}^{-1})_N(0f)_\Lambda]_{J=6^+}$$

configuration at $E_\Lambda=8.5$ MeV. The

$$[(0f_{5/2}^{-1})_N(0l)_\Lambda]_{J=\max}$$

series is also sizably excited, but this series is not expected to be peaked because of the considerable spreading width of the neutron $0f_{5/2}$-hole state.

The obtained peaks can be compared with the observed data of the ^{89}Y$(\pi^+,K^+)^{89}_{\Lambda}$Y reaction[8] with $p_\pi=1050$ MeV/c, since the sample nucleus ^{90}Zr has also the $0g_{9/2}$-neutron closed shell and a proton hole in ^{89}Y does not change the situation if the strengths are summed up over the final-state angular momenta. In fact, we see three clear peaks at

$$E_\Lambda^{\rm exp}\approx -16,\ -9,\ \text{and}\ -1.5\ \text{MeV}$$

and the ground-state signal around $E_\Lambda^{\rm exp}=-23$ MeV in the experimental spectrum. Thus the calculated series is in reasonable agreement with the observed peaks. Moreover, it will be interesting to compare the predicted high-spin resonance and QF behavior with the experimental one in the continuum at $E_\Lambda>5$ MeV.

The forward-angle effective numbers for the above four peaks are calculated in DWIA and listed in Table III. Experimentally[8] only the ground-state cross section is reported to be 0.6 μb/sr at $\theta=10°$. Considering some reduction depending on θ, the calculated value for $\theta=0°$,

$$\frac{d\sigma}{d\Omega}[0g_{9/2N}^{-1}0s_\Lambda]=1.7\ \mu\text{b/sr}\ (\theta=0°)\ ,$$

seems to be reasonable in spite of the simple treatment. This is due to the fact that the target wave function is represented with the $0g_{9/2}$ closed one to a good approximation.

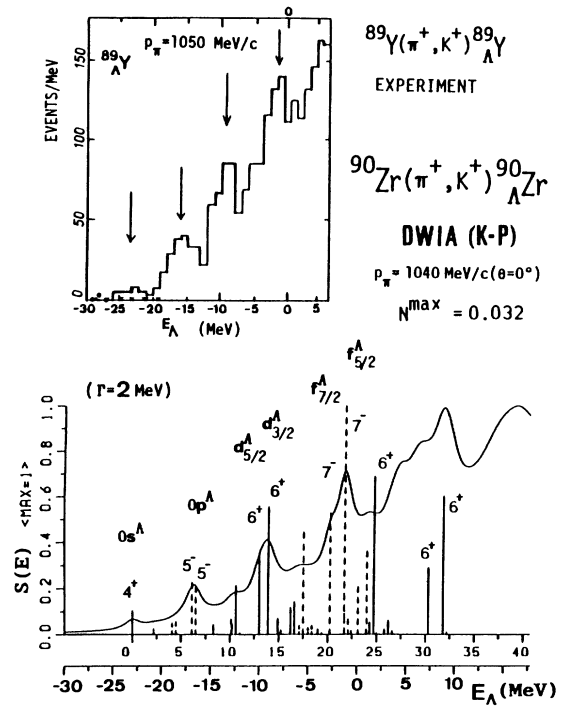

FIG. 6. Calculated strength functions $S_\Gamma(E_\Lambda;\theta=0°)$ for the ^{90}Zr$(\pi^+,K^+)^{90}_{\Lambda}$Zr reaction (K-P method), where Lorentzian width of $\Gamma=2$ MeV is employed for surface neutron-hole orbits. For the deeper orbits below $0f_{5/2}$, $\Gamma=4$ MeV Lorentzian is used. For reference, the experimental spectrum (Ref. 8) for the ^{89}Y$(\pi^+,K^+)^{89}_{\Lambda}$Y reaction is compared. Comments are the same as for Fig. 4.

C. The $^{40}Ca(\pi^+,K^+)^{40}_{\Lambda}Ca$ reaction

In the $^{40}Ca(\pi^+,K^+)^{40}_{\Lambda}Ca$ experiment[8] the observed spectrum does not seem to show such a clear series of peaks as in other cases. Apart from the experimental resolution, this is partly due to the unfavorable fact that the target is *LS* closed. In fact, Chrien[8] has suggested the expected configurations in the observed spectrum as indicated in the top of Fig. 7. Here we show how the (π^+,K^+) spectrum depends on the peripheral neutron spin-orbit splitting by changing the value

$$\Delta=\varepsilon(d_{3/2N})-\varepsilon(d_{5/2N})$$

around the empirical one ($\Delta^{exp}\approx 5.5$ MeV).

Figure 7 displays three calculated spectra with $\Delta=4.5$ MeV, 5.5 MeV(exp), and 7.0 MeV, where the effective neutron numbers are folded with Lorentzian of width $\Gamma=3$ MeV. In the calculations, we obtain two series of strongly excited peaks in the $^{40}Ca(\pi^+,K^+)^{40}_{\Lambda}Ca$ spectrum. One is the $d_{3/2N}$-hole series consisting of three peaks with Λ being in the 0*s*, 0*p*, and 0*d* orbits, respectively,

$$[(0d_{3/2}^{-1})_N 0s_\Lambda]_{J=2^+},$$

$$[(0d_{3/2}^{-1})_N 0p_\Lambda]_{3^-},$$

$$[(0d_{3/2}^{-1})_N 0d_\Lambda]_{4^+}.$$

They are indicated by triangles in Fig. 7. The other is the corresponding $d_{5/2N}$-hole series with $J=2^+$, 3^-, and 4^+,

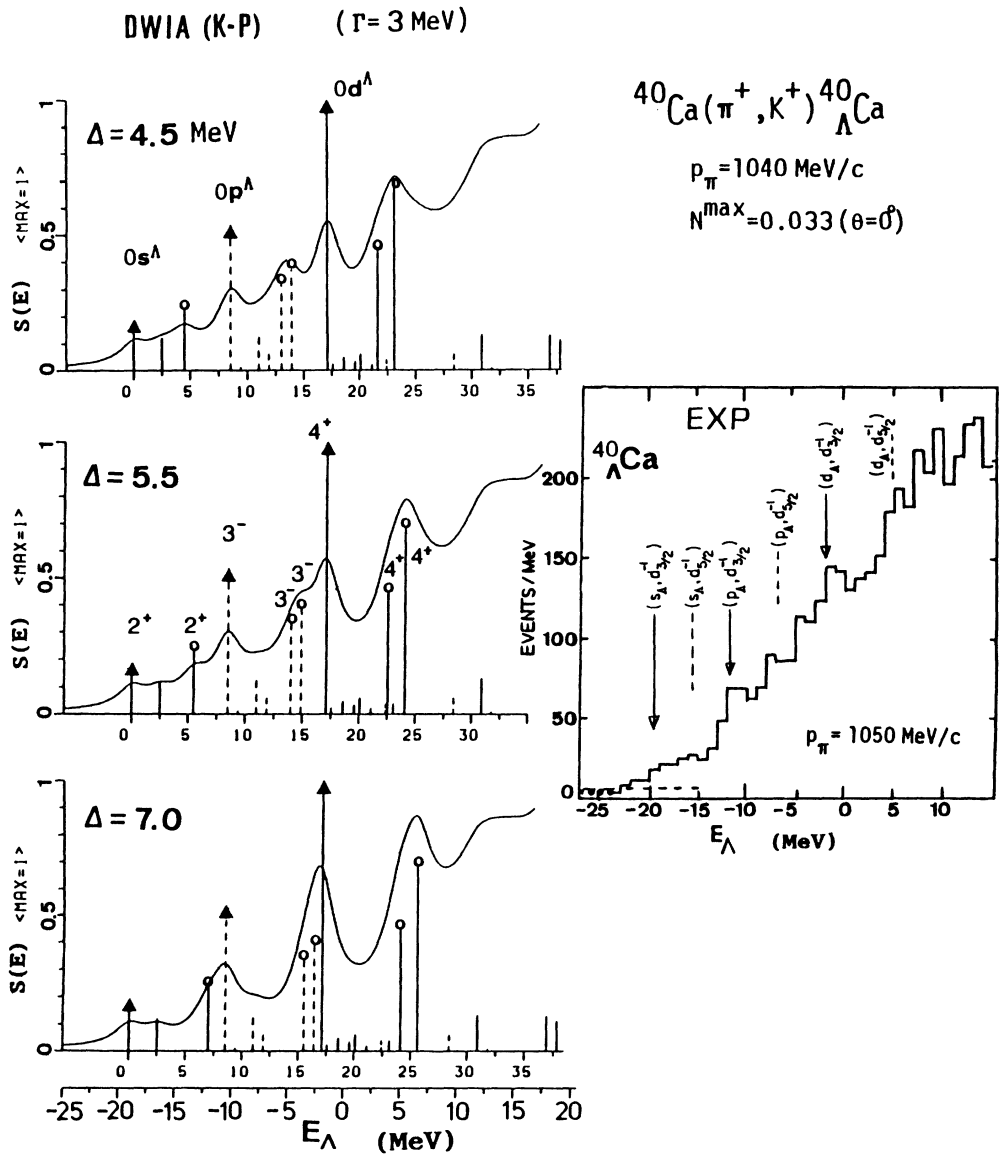

FIG. 7. Change of the K-P calculated strength function $S_\Gamma(E_\Lambda;\theta=0°)$ for $^{40}Ca(\pi^+,K^+)^{40}_{\Lambda}Ca$ as a function of the neutron $0d_{5/2}^{-1}-0d_{3/2}^{-1}$ splitting Δ. The lines with triangles indicate the strengths for $[0d_{3/2}^{-1}j_\Lambda]$ and those with open circles for $[0d_{5/2}^{-1}j_\Lambda]$. Lorentzian width $\Gamma=3$ MeV is used in the folding. The experimental spectrum with the suggested structures is taken from Ref. 8.

as marked by open circles. The obtained major shell interval for Λ is $\hbar\omega_\Lambda \approx 8.5$ MeV, which is reflected in the 2^+-3^--4^+ spacings within each series.

It is easily understood from the above relation of the energy spacings that, if $\Delta < 5.5$ MeV, the two series tend to fill in the valleys with each other as shown in the upper two theoretical spectra. On the other hand, if $\Delta > 6$ MeV, the 3^- and 4^+ peaks belonging to the $d_{3/2N}$-hole series just overlap with the members in the $d_{5/2N}$-hole series within 1.5 MeV distance and as a result we get well-separated peak spectrum as shown in the insertion with $\Delta = 7.0$ MeV. It should be noted that the experimental situation of the neutron spin-orbit splittings points at the former case ($\Delta^{\rm exp} \approx 5.5$ MeV), and hence one can understand qualitatively why rather unclear peaks in the experimental $^{40}\mathrm{Ca}(\pi^+,K^+)^{40}_\Lambda\mathrm{Ca}$ spectrum appear only.

If the experimental resolution is improved, the two series of peaks will be observed more distinctly even in this "heavy" LS-closed target case. In fact the corresponding peaks can be identified in the LS-closed $^{16}\mathrm{O}(\pi^+,K^+)^{16}_\Lambda\mathrm{O}$ case as will be shown below. Thus the peak density of the (π^+,K^+) reaction on the LS-closed target depends sensitively on the mutual relation between the peripheral neutron spin-orbit splitting Δ and the Λ major-shell distance $\hbar\omega_\Lambda$.

D. The $^{28}\mathrm{Si}(\pi^+,K^+)^{28}_\Lambda\mathrm{Si}$ reaction

As for the $^{28}\mathrm{Si}(\pi^+,K^+)^{28}_\Lambda\mathrm{Si}$ reaction, the K-P result ($\theta = 0°$, $\Gamma = 2$ MeV) and the CSM result ($\theta = 10°$, $\Gamma = 3$ MeV) are shown in Figs. 8 and 9, respectively. The difference in their transferred momenta due to the kinematical condition is not large. Both methods give a similar pattern of spectra, since the third peak obtained at $E_\Lambda \approx 4$ MeV in the CSM spectrum (Fig. 9) becomes clearer if smaller Lorentzian width $\Gamma = 2$ MeV is used as in Fig. 8.

As far as the pattern of the spectrum is concerned, it may be justified to simply assume the target to be $0d_{5/2}$ closed, because the largest angular momentum orbit near the surface plays a major role and also because admixtures of other components in the target wave function affect the absolute magnitudes of the strengths only.

The observed excitation function[8] is compared in Fig. 8 where the correspondence between the two spectra is rather good in their peak energies and relative heights. Three clear peaks are attributed to the following structures:

$$[0d^{-1}_{5/2N}(nl)_\Lambda]_J$$

with

$$nl_\Lambda(J) = 0s_\Lambda(2^+_{\rm g.s.})$$

at

$$E^{\rm cal}_\Lambda = -16.8 \text{ MeV } (E^{\rm exp}_\Lambda \approx -16 \text{ MeV}),$$

$$(0p_{3/2} \text{ and } 0p_{1/2})_\Lambda(3^-)$$

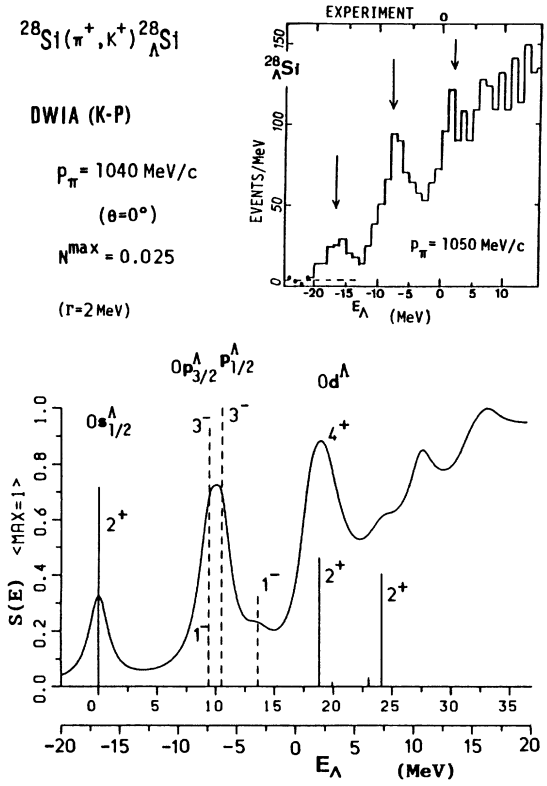

FIG. 8. The K-P result for the strength function $S_\Gamma(E_\Lambda;\theta=0°)$, $\Gamma = 2$ MeV Lorentzian, for the $^{28}\mathrm{Si}(\pi^+,K^+)^{28}_\Lambda\mathrm{Si}$ reaction is compared with the experimental spectrum (Ref. 8). Comments are the same as for Fig. 4.

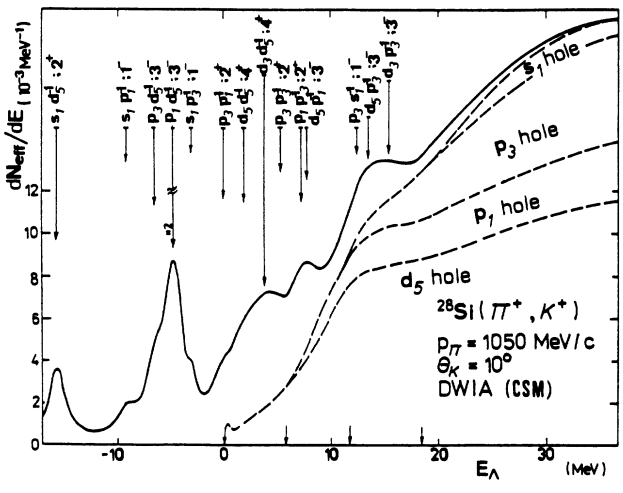

FIG. 9. The CSM result of the strength function $S_\Gamma(E_\Lambda;\theta=10°)$, $\Gamma = 3$ MeV Lorentzian, for the $^{28}\mathrm{Si}(\pi^+,K^+)^{28}_\Lambda\mathrm{Si}$ reaction with $p_\pi = 1050$ MeV/c. To show the dominant p-h structure $[j_\Lambda j_N^{-1}];J$, the notations are used as d_5 for $0d_{5/2}$, p_3 for $0p_{3/2}$, etc. See also the caption of Fig. 5.

at

-7.4 and -6.3 MeV (-7 MeV),

$0d_\Lambda(4^+$ resonance) at 2.0 MeV (2 MeV),

where the last peak originates from two sharp resonances just above the Λ threshold and the broad "bound-state peak" of

$$[(0p_{1/2}^{-1})_N(0p_{3/2})_\Lambda]_{J=2^+}\ .$$

The good correspondence indicates that the adopted Woods-Saxon potential for Λ works reasonably well and that the Λ major-shell interval in this mass region is $\hbar\omega_\Lambda \approx 9$ MeV. The DWIA cross section for the ground-state 2^+ peak at forward angle is estimated to be

$$\frac{d\sigma}{d\Omega}[0d_{5/2N}^{-1}0s_\Lambda]=8.9\ \mu\text{b/sr}\quad(\theta=0^\circ)\ .$$

Chrien[8] reported the experimental cross section for this state at $\theta=10^\circ$ to be 1.8 μb/sr. The cross section at $\theta=10^\circ$ becomes ≈50% of the above value, however it still remains about three times larger than the observed value. The remedy for this discrepancy may be achieved by improving further the transition operator and also the target wave function which is simply assumed here to be $d_{5/2}$ closed. It is remarked that the $d_{5/2}$ neutron occupation number in the ^{28}Si ground state is experimentally 3.6–4.5 (i.e., 60–75 % $d_{5/2}$ closure).[26]

E. The $^{16}O(\pi^+,K^+)^{16}_\Lambda O$ reaction

Comparison is made in Fig. 10 for the experimental spectrum[8] and the K-P result ($\theta=0^\circ$, $\Gamma=2$ MeV) of the $^{16}O(\pi^+,K^+)^{16}_\Lambda O$ reaction. Theoretical spectra (the CSM one is to be found in Ref. 21) show a very good correspondence to the experimental four peaks. They are reasonably characterized by the following structures:

$[0p_{1/2N}^{-1}0s_\Lambda]_{J=1^-_{g.s.}}$ at $E_\Lambda^{cal}=-13.0$ MeV

$(E_\Lambda^{exp}\approx -13$ MeV),

$[0p_{3/2N}^{-1}0s_\Lambda]_{J=1^-}$ at -6.9 MeV (-6 MeV),

$[0p_{1/2N}^{-1}0p_{3/2\Lambda}]_{J=2^+}$ at -2.7 MeV (-2.5 MeV),

$[0p_{3/2N}^{-1}0p_\Lambda]_{J=2^+}$ resonance at 4 MeV (5 MeV).

The last 2^+ peak consists of two sharp resonances at $E_\Lambda=3.4$ and 4.6 MeV in the continuum. The observed width of the last peak is about 2 MeV and this gives a restriction to the Λ spin-orbit potential. In this respect the value $V_{SO}^\Lambda=2.0$ MeV employed in the present calculation seems to be an acceptable upper limit. The reaction cross sections for the above four peaks are estimated in DWIA, from $1^-_{g.s.}$ upwards, as

$$\frac{d\sigma}{d\Omega}(\theta=0^\circ)=4.9,\ 8.5,\ 10.6,\ 17.6\ \mu\text{b/sr}\ .$$

Some of these values are not much different from the previous harmonic oscillator estimates by Dover *et al.*[5]

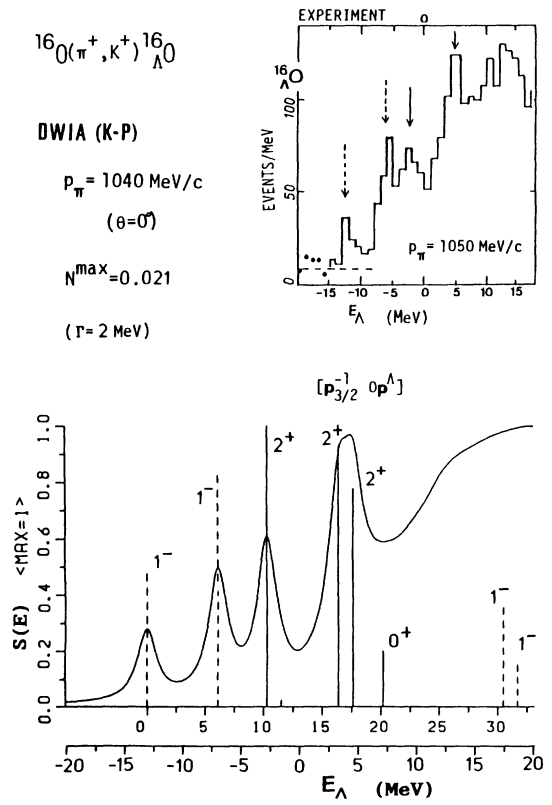

FIG. 10. The K-P result of the strength function $S_\Gamma(E_\Lambda;\theta=0^\circ)$, $\Gamma=2$ MeV Lorentzian, and the experimental spectrum (Ref. 8) for the $^{16}O(\pi^+,K^+)^{16}_\Lambda O$ reaction. Comments are the same as for Fig. 4.

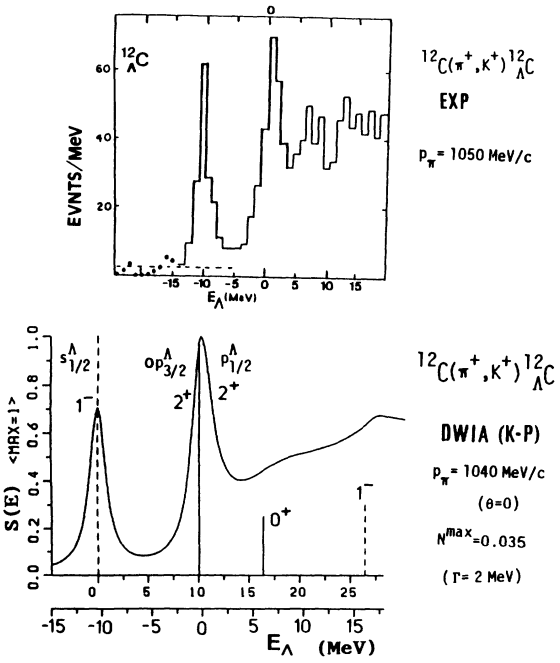

FIG. 11. The K-P result of the strength function $S_\Gamma(E_\Lambda;\theta=0^\circ)$, $\Gamma=2$ MeV Lorentzian, and the experimental spectrum (Ref. 8) for the $^{12}C(\pi^+,K^+)^{12}_\Lambda C$ reaction. Comments are the same as for Fig. 4.

(with h.o. size $b=1.71$ fm and $p_\pi=1100$ MeV/c).

Four peaks of the same p-h combinations were first found in the $^{16}O(K^-,\pi^-)^{16}_{\Lambda}O$ reaction.[1] In the present (π^+,K^+) case, because of the sizable transferred momentum, the last two peaks are not the substitutional 0^+ states but the "high-spin" 2^+ states, and the first two 1^- states are excited relatively more strongly and more clearly than in the (K^-,π^-) case.

F. The $^{12}C(\pi^+,K^+)^{12}_{\Lambda}C$ reaction

Figure 11 displays the calculated strength functions for $^{12}C(\pi^+,K^+)^{12}_{\Lambda}C$ reaction in comparison with the recent experiment.[8] The agreement between the two spectra is good. The two clear peaks are well known to have the structures

$$[(0p_{3/2}^{-1})_N(0s_{1/2})_\Lambda]_{J=1^-_{\text{g.s.}}} \text{ at } E_\Lambda^{\text{cal}}=-10.4 \text{ MeV}$$

$$(E_\Lambda^{\text{exp}}=-10.5 \text{ MeV}),$$

$$[(0p_{3/2}^{-1})_N(0p)_\Lambda]_{J=2^+} \text{ at } 0.0 \text{ MeV } (0.5 \text{ MeV}).$$

In the present DWIA calculation, we get the ground-state (π^+,K^+) cross sections:

$$\frac{d\sigma}{d\Omega}[0p_{3/2N}^{-1}0s_\Lambda]_{1^-}=17.4(\theta=0°),\ 14.1(\theta=5°),\ 8.4(\theta=10°)\ \mu\text{b/sr}.$$

These values are in good agreement with the experimental cross sections 12 μb/sr($\theta=5.6°$) and 8.5 μb/sr($\theta=10.3°$).[6] For the second peak we obtain

$$\frac{d\sigma}{d\Omega}[0p_{3/2N}^{-1}0p_\Lambda]=23.7(\theta=0°),\ 21.3(\theta=5°),\ 15.2(\theta=10°)\ \mu\text{b/sr}.$$

The results are consistent with the observed value 17 μb/sr ($\theta=5.6°$).[6]

Halderson *et al.*[14] have obtained an analogous DWIA strength function by employing a version of CSM and the Cohen-Kurath–type wave functions. There, however, too much structure with pronounced dips is obtained in the region above the threshold $E_\Lambda=0$, also their ratio between the peak strength and QF part differs appreciably from the situation depicted in Fig. 11.

G. The $^9Be(\pi^+,K^+)^9_{\Lambda}Be$ reaction

Chrien[8] also reported data on the (π^+,K^+) production of $^9_{\Lambda}$Be. In the preceding cases (A–F), the single-particle aspect dominates in their structures, while the cluster aspect plays an important role in such light systems as $^9_{\Lambda}$Be. In fact the data disclose several bands of levels including genuine hypernuclear states. Here we only mention that this new (π^+,K^+) data as well as the (K^-,π^-) spectrum can be well described by the extended microscopic cluster model.[10,27]

V. CONCLUDING REMARKS

In view of the new and wide range of experimental data on the (π^+,K^+) hypernuclear production,[8] we have extended the DWIA calculation of the strength functions so as to include the continuum effects, resonances and quasi-free contributions, and hence to allow the realistic comparison with the experimental data. The continuum effects are evaluated by the Kapur-Peierls method and also by the continuum shell model.

The most noticeable characteristic of the (π^+,K^+) reaction lies in its striking selectivity which is indeed desirable to observe full series of hyperon single-particle orbits even in heavy hypernuclei. This is an important complement to the in-flight (K^-,π^-) reaction which selects the substitutional states only. The selective nature of the (π^+,K^+) reaction, which provides well-separated series of peaks, has been found to persist after the continuum effects are taken into account. Even a resonant peak in the continuum can remain quite narrow just because of its structure pertinent to the (π^+,K^+) selectivity.

The basic structure input which we have employed in the present calculation is simple [N-hole Λ-particle] configurations. In reality, the wave functions of the target nucleus and the produced hypernucleus should be more complicated with substantial configuration mixings and spreadings of the single-particle strengths. For example, the calculated cross sections may change by a factor of some 2, if more realistic wave functions are used. The contact residual interaction in CSM does not change appreciably the pattern of the spectra. The calculated (π^+,K^+) strength functions show quite a good correspondence to the observed data[8] for mass 12–89 hypernuclei. The reason should be again in the (π^+,K^+) selectivity which favors a particular [N-hole Y-particle] configuration with stretched angular momentum J. Another reason is, of course, in the instrumental resolution of measurements. Usefulness of its improvement has been demonstrated. If the absolute magnitude of the cross section and/or more detailed structure of the excitation function come into discussion after new experiments, we can improve our calculation further.

The Woods-Saxon potential with 30 MeV depth reproduces the observed Λ single-particle spectra in mass 12–89 hypernuclei within experimental uncertainty of about 3 MeV consistently with the early analyses of B_Λ in light hypernuclei. This seems to imply the success of the local potential for Λ. The nonlocality in the Λ single-particle potential U_Λ can arise from the ΛN exchange interaction due to strange-meson exchanges and from ΛNN forces, and also from the ΛN short-range correlations in

medium, although there is no Fock term. However, the nonlocality in U_Λ is considered to be much weaker than in the nucleon potential U_N (Ref. 28) and therefore it is too early to conclude the locality of U_Λ with use of the present accuracy of the experimental data. In view of the apparent success of the Woods-Saxon potential for Λ and of the comparison with the nuclear case, Dover[29] made a discussion on distinguishability or indistinguishability of Λ and nucleon and on the possibility of the partial quark deconfinement deep inside the nucleus. In order to make a realistic discussion on such a problem, however, it will be necessary to extend and refine both theoretical and experimental investigations.

The (π^+,K^+) reaction appears thus at present to be a very powerful method of hypernuclear production both theoretically and experimentally. Its usefulness is not only for revealing hyperon deep orbits but also for more general hypernuclear spectroscopy.

Note added in proof. As the experimental data taken from Ref. 8 are preliminary, the readers should refer to the final version which will be published in due time. The authors are grateful to P. H. Pile for remarking this point and also for discussion.

ACKNOWLEDGMENTS

The authors would like to express their sincere thanks to R. E. Chrien for fruitful conversation on the recent (π^+,K^+) results. They are also grateful to H. Ejiri, T. Fukuda, O. Hashimoto, K. Ikeda, K. Nakai, T. Shibata, T. Yamada, T. Yamazaki, and K. Yazaki for useful discussions. One of the authors (J.Ž.) is obliged to the Institute for Nuclear Study (INS) of University of Tokyo, the Research Institute for Fundamental Physics (RIFP) of Kyoto University, Fukui University, and Osaka Electro-Communication University for support which made the start of the present collaboration possible.

[1]W. Brückner *et al.*, Phys. Lett. **55B**, 107 (1975); **62B**, 481 (1976); **79B**, 157 (1978); R. Bertini *et al.*, Nucl. Phys. **A360**, 315 (1981); B. Povh, Rep. Prog. Phys. **39**, 824 (1976); Annu. Rev. Nucl. Part. Sci. **28**, 1 (1978).

[2]Proceedings of the International Symposium on Hypernuclear and Kaon Physics, Brookhaven, 1985, edited by R. Chrien [Nucl. Phys. **A450** (1986)].

[3]T. Yamazaki *et al.*, Phys. Lett. **144B**, 177 (1984); Phys. Rev. Lett. **54**, 102 (1985).

[4]J. Hüfner, S. Y. Lee, and H. A. Weidenmüller, Nucl. Phys. **A234**, 429 (1974); Phys. Lett. **49B**, 409 (1974); A. Bouyssy, Nucl. Phys. **A290**, 324 (1977); R. H. Dalitz and A. Gal, Ann. Phys. **116**, 167 (1978).

[5]C. B. Dover, L. Ludeking, and G. E. Walker, Phys. Rev. C **22**, 2073 (1980).

[6]C. Milner *et al.*, Phys. Rev. Lett. **54**, 1237 (1985).

[7]H. Bandō and T. Motoba, Prog. Theor. Phys. **76**, 1321 (1986).

[8]R. E. Chrien, Brookhaven National Laboratory Report BNL 39723, 1987; Proceedings of the XI International Conference on Particles and Nuclei, PANIC'87, Kyoto, 1987 [Nucl. Phys. **A478**, 705c (1988)].

[9]H. Ejiri, T. Shibata, T. Fukuda, H. Bandō, and K.-I. Kubo, Phys. Rev. C **36**, 1435 (1987).

[10]H. Bandō, Proceedings of the XI International Conference on Particles and Nuclei, PANIC'87, Kyoto, 1987 [Nucl. Phys. **A478**, 697c (1988)].

[11]T. Motoba, Proceedings of the International Symposium on Strangeness in Hadronic Matter, Bad Honnef, Federal Republic of Germany, 1987 [Nucl. Phys. **A479**, 227c (1988)].

[12]C. Mahaux and H. A. Weidenmüller, *Shell Model Approach to Nuclear Reactions* (North-Holland, Amsterdam, 1969); H. W. Barz, I. Rotter, and J. Höhn, Nucl. Phys. **A275**, 111 (1977).

[13]R. Wünsch, L. Majling, and J. Žofka, Czech. J. Phys. **B36**, 441 (1986).

[14]D. Halderson, Y. Mo, and P. Ning, Phys. Rev. Lett. **57**, 1117 (1986).

[15]T. Kishimoto, Nucl. Phys. **A450**, 445c (1986); R. E. Chrien, E. V. Hungerford, and T. Kishimoto, Phys. Rev. C **35**, 1589 (1987).

[16]O. Morimatsu and K. Yazaki, Nucl. Phys. **A435**, 727 (1985); Proceedings of the 1986 INS Symposium on Hypernuclear Physics, edited by H. Bandō, K. Ogawa, and H. Hashimoto, Tokyo, 1986 (INS, University of Tokyo, 1986), p. 50.

[17]R. Hausmann and W. Weise, Z. Phys. A **324**, 355 (1986); M. Kohno, R. Hausmann, P. Siegel, and W. Weise, Nucl. Phys. **A470**, 609 (1987).

[18]J. Žofka, Proceedings of the 1986 INS Symposium on Hypernuclear Physics, edited by H. Bandō, K. Ogawa, and H. Hashimoto, Tokyo, 1986 (INS, University of Tokyo, 1986) p. 97; R. Wünsch and J. Žofka, Phys. Lett. **193B**, 7 (1987).

[19]H. Bandō, T. Motoba, and J. Žofka, Z. Phys. **A330**, 203 (1988).

[20]P. L. Kapur and R. E. Peierls, Proc. R. Soc., London **A166**, 277 (1938); A. M. Lane and D. Robson, Phys. Rev. **151**, 774 (1966); **161**, 982 (1967); **185**, 1403 (1969); C. Bloch, Nucl. Phys. **4**, 503 (1957).

[21]T. Motoba, H. Bandō, R. Wünsch, and J. Žofka, Osaka Electro-Communication University Report OECU-1987-12, 1987.

[22]European Organization for Nuclear Research Report No. CERN/HERA 72-1 (1975) and 75-1 (1975).

[23]E. H. Auerbach, A. J. Baltz, C. B. Dover, A. Gal, S. H. Kahana, L. Ludeking, and D. J. Millener, Ann. Phys. (N.Y.) **148**, 381 (1983).

[24]O. Hashimoto *et al.*, private communication.

[25]J. Žofka, M. Sotona, and V. N. Fetisov, Nucl. Phys. **A431**, 603 (1984).

[26]P. M. Endt and C. Van Der Leun, Nucl. Phys. **A310**, 1 (1978).

[27]T. Yamada, K. Ikeda, H. Bandō, and T. Motoba, Proceedings of the International Conference on The Theory of Few-Body and Quark-Hadronic Systems, Dubna, 1987 (JINR, Dubna, 1987); Phys. Rev. C **38**, 854 (1988).

[28]H. Bandō and S. Nagata, Prog. Theor. Phys. **67**, 522 (1982).

[29]C. Dover, Talk at the International Symposium on Medium Energy Physics, Beijing, 1987, Brookhaven National Laboratory Report BNL 40074, 1987.